RSC Advances

PAPER

View Article Online
View Journal | View Issue

Check for updates

Cite this: *RSC Adv.*, 2025, **15**, 10144

Synthesis of core/shell cobalt-doped rutile TiO_2 nanorods for MB degradation under visible light†

Lang Yang,[a] Jialei Ying,[a] Zhenzhong Liu, *[a] Guangyu He,[b] Linli Xu,[c] Mingyue Liu, [c] Xinlei Xu,[a] Guihua Chen[c] and Meili Guan*[d]

Although TiO_2 has been widely applied in many fields, the design and preparation of one-dimensional rutile TiO_2 nanomaterials for high-efficiency photocatalysis under visible light remain challenging. Herein, uniform Co-doped rutile TiO_2 nanorods with selective adsorption and photocatalytic activity for methylene blue (MB) have been developed *via* a one-pot molten salt flux method. Compared to pure rutile TiO_2 nanorods, the Co-doped rutile TiO_2 nanorods exhibited an obvious core/shell structure with smaller inner crystal face spacing (d_{001} = 0.20 nm) and a larger rough surface (the BET specific surface area is 25 m^2 g^{-1}). Furthermore, different dyes were employed to investigate the adsorption ability of Co-doped rutile TiO_2 nanorods. The density functional theory (DFT) calculations determined that both the electrostatic potential and molecular structure could influence the adsorption behavior on the photocatalyst surface. The results indicated that the Co-doped TiO_2 nanorods possessed a high selective adsorption capacity for MB (134.54 mg g^{-1} in neutral solution). The degradation of MB using Co-doped rutile TiO_2 nanorods was conducted under visible light irradiation, yielding with an apparent rate constant of 0.301 min^{-1} at pH = 7. The degradation mechanism was further explored through electron spin resonance (ESR) experiments, which identified the formation of superoxide anions ($\cdot O_2^-$) and hydroxyl radicals ($\cdot$OH) in the system. This study provides a new strategy for preparing novel rutile TiO_2 photocatalysts for the degradation of organic dyes under visible light.

Received 15th December 2024
Accepted 14th March 2025

DOI: 10.1039/d4ra08773a

rsc.li/rsc-advances

Open Access Article. Published on 02 April 2025. Downloaded on 4/29/2026 6:45:28 AM.
This article is licensed under a Creative Commons Attribution-NonCommercial 3.0 Unported Licence.

Introduction

With the rapid development of global industry, the problem of environmental pollution has become increasingly evident. Many organic pollutants in water are toxic and difficult to degrade, which damages the ecological environment and endangers human health. Traditional methods for treating organic pollutants, such as physical,[1,2] chemical,[3,4] and biochemical[5,6] approaches, often entail high costs and produce unsatisfactory results. Nowadays, photocatalysis[7,8] has emerged as a promising solution for water treatment. This technology utilizes light to generate free radicals with strong oxidative properties, effectively breaking down organic pollutants in wastewater.

Among semiconductor materials, titanium dioxide (TiO_2)[9,10] stands out as one of the most significant photocatalysts for wastewater treatment due to its low cost, non-toxicity, and stability. TiO_2 mainly exists in three crystalline polymorphs: anatase,[11,12] rutile,[13,14] and brookite.[15] The properties of TiO_2 are highly dependent on its shape and crystal phase, which influence the adsorption and activation of target molecules. Numerous studies have focused on the photocatalytic degradation of organic pollutants using rutile TiO_2. For example, Guan *et al.* reported a highly efficient rutile/brookite homojunction that enhanced photocatalytic activity for hydrogen generation and organic dye degradation through precise control of the crystal phase.[16] Djokić *et al.* obtained a nanocrystalline rutile TiO_2 *via* a low-temperature process, the photocatalytic degradation process of reactive orange 16 was completed 2.6 times faster.[17] Despite these advancements, rutile TiO_2 generally has a relatively high energy bandgap (3.2 eV), leading to lower efficient photocatalytic properties. This limitation hinders its broader application, highlighting the need for further research and modifications to enhance its performance.

Recently, one dimensional (1D) TiO_2 nanomaterials, including nanorods,[18] nanotubes,[19] and nanoarrays,[20] have garnered significant attention due to their unique structures and properties. However, these materials can only be activated by UV light. Doping TiO_2 with various atoms has proven to be an

[a]*Taizhou Key Laboratory of Medical Devices and Advanced Materials, Taizhou Institute of Zhejiang University, Taizhou 318000, China. E-mail: zzliu@zju.edu.cn*
[b]*Department of Chemistry, School of Science and Research Center for Industries of the Future, Westlake University, Hangzhou 310030, China*
[c]*School of Pharmaceutical and Chemical Engineering, Taizhou University, Taizhou 318000, China*
[d]*College of Chemical and Biological Engineering, Shandong University of Science and Technology, Qingdao 266590, China. E-mail: mlguan@sdust.edu.cn*

† Electronic supplementary information (ESI) available. See DOI: https://doi.org/10.1039/d4ra08773a

© 2025 The Author(s). Published by the Royal Society of Chemistry

Open Access Article. Published on 02 April 2025. Downloaded on 4/29/2026 6:45:28 AM. This article is licensed under a Creative Commons Attribution-NonCommercial 3.0 Unported Licence.

effective strategy for extending its absorption from the UV to the visible region,[21,22] thereby enhancing its photocatalytic activity under visible light. For example, Lv *et al.* reported the synthesis of thiourea-modified TiO_2 nanorods, where the N-doped TiO_2 nanorods exhibited increased photocatalytic activity for the degradation of rhodamine B (RhB) under visible light.[23] Similarly, Ide *et al.* synthesized a rutile TiO_2 nanobundle that demonstrated superior visible light-responsive photocatalytic activity for the removal of formic acid in water.[24] Despite these advancements, the activity of rutile TiO_2 still requires further enhancement for practical applications.

Herein, we report the synthesis of novel cobalt-doped rutile TiO_2 nanorods with controllable morphologies and enhanced functional properties, achieved through a simple one-pot molten salt flux method. This unique nanostructure endows the rutile TiO_2 nanorods with a high surface area and excellent visible light utilization, resulting in high-efficiency adsorption and photocatalytic activity under visible light for the degradation of methylene blue (MB). Consequently, we aim to explore novel and highly efficient photocatalysts for wastewater treatment.

Experimental

Materials

Titanium dioxide (P25, Degussa), sodium chloride (NaCl, Sigma-Aldrich), sodium dihydrogenphosphate (Na_2HPO_4, Sigma-Aldrich), cobalt nitrate hexahydrate ($CoH_{12}N_2O_{12}$, Energy), Methylene Blue (MB, Aladdin), Neutral Red (NR, Sinoreagent), Rhodamine B (RhB, TCI), Methyl Orange (MO, Aladdin), Brilliant Blue (BB, Macklin), Cresol Red (CR, Shzychem), and acetonitrile (C_2H_3N, Aladdin). 2,2,6,6-Tetramethylpiperidino-1-oxy (TEMPO) and 5,5-dimethyl-1-pyrroline-N-oxide (DMPO) were obtained from Aladdin.

Synthesis of core/shell Co-doped TiO_2 nanorods

A mixture of P25 (1 g), NaCl (4 g), Na_2HPO_4 (1 g), and cobalt nitrate (100 mg) was put in a mortar and thoroughly ground. The mixture was calcined in a tubular furnace at a heating rate of 10 °C min^{-1} up to 825 °C for 6 hours. After cooling to room temperature, the impurities were removed by boiling the product with deionized water. Finally, the Co-doped TiO_2 nanorods were obtained by drying the material in an oven at 60 °C. As a contrast, pure TiO_2 nanorods were obtained without adding cobalt nitrate.

Adsorption study of Co-doped rutile TiO_2 nanorods

In order to study the selective adsorption ability of Co-doped nanorods in neutral water, six different dyes were used. Specifically, 5 mg Co-doped nanorods were added to 30 mL, 20 mg L^{-1} of different dye solutions, which was magnetically stirred for 1 hour. After centrifugated to remove the photocatalyst, UV-Vis spectrophotometer was used to measure the adsorption capacity of Co-doped TiO_2 nanorods for different dyes. In order to further investigate the adsorption of MB in different pH values (*e.g.* pH = 3, 5, 7 and 9), HCl or NaOH was used to adjust the acidity and alkalinity of MB solution. The amount of MB dye adsorbed was calculated using the following equation:

$$q_e = (C_0 - C_e) \times V/m$$

where q_e is the adsorption capacity (mg g^{-1}), C_0 is the initial concentration of dye (mg L^{-1}), C_e is the equilibrium concentration of dye (mg L^{-1}), V is the volume of the solution (L), and m is the mass of adsorbent (g). Finally, quantum chemical calculations were used to explore the mechanism of adsorption. The electrostatic potential and size were obtained with Multiwfn.[25–27]

Photocatalytic performance of Co-doped rutile TiO_2 nanorods

The photocatalytic activity of Co-doped TiO_2 nanorods was evaluated by the degradation of MB solution using a 240 W Xe lamp system in a black box (XW-GHX-IV), which was equipped with 8 Quartz test tubes and a cutoff filter (λ > 420 nm). The energy intensity was set at 200 mW cm^{-2}. Before reaction, 5 mg catalyst was added into 60 mL, 20 mg L^{-1} MB solution and stirred in the dark for 90 min to achieve adsorption equilibrium. During the dark reaction, 3 mL of the suspension was taken every hour and centrifuged to remove the photocatalyst. To enhance degradation efficacy, a considerable amount of H_2O_2 (15 μL) was added to the light-irradiated mixture.[28,29] Subsequently, 3 mL of the suspension was taken every hour and centrifuged to remove the photocatalyst. The concentration of MB was analyzed using UV-Vis absorption measurements, determined by its characteristic absorption peak at 662 nm. The rate constant (k) was calculated by the following equation:

$$\ln C_t/C_0 = k_t$$

where C_0 and C_t represent the concentration of MB at the initial time and after t hour, respectively. k represents the rate constant. The recyclability and stability of Co-doped rutile TiO_2 nanorods were investigated. The collected powder was treated with H_2O_2 for a certain time, then washed with ethanol and water, followed by centrifugation and drying under vacuum. The recycled photocatalyst was directly used in subsequent experiments. This recycling process was repeated five times. Additionally, the photocatalytic degradation of MB at different pH values (*e.g.*, pH = 3, 5, 7, and 9) was investigated. Finally, the catalytic degradation of the MB solution with different catalyst concentrations (*e.g.*, 1 mg, 3 mg, 5 mg, and 7 mg) was also examined.

Reactive species identification of TiO_2 nanorods

The reactive oxygen species (ROS) generated by Co-doped TiO_2 nanorods were identified using an electron spin resonance (ESR) spectrometer. Typically, photogenerated holes (h^+) and photogenerated electrons (e^-) were detected by mixing a suspension of Co–TiO_2 nanorods (200 μL, 1.0 mg mL^{-1}) with TEMPO (200 μL, 30 mM) in acetonitrile. The hydroxyl radical (·OH) was identified by mixing the catalyst suspension (200 μL, 1.0 mg mL^{-1}) with DMPO (200 μL, 100 mM) in water. The

Open Access Article. Published on 02 April 2025. Downloaded on 4/29/2026 6:45:28 AM. This article is licensed under a Creative Commons Attribution-NonCommercial 3.0 Unported Licence.

superoxide radical ($\cdot O_2^-$) was detected by mixing the catalyst suspension (30 μL, 1.0 mg mL^{-1}) with DMPO (200 μL, 100 mM) in methanol. The resulting mixture was transferred to a capillary tube and placed into the EPR sample chamber for reactive species analysis. This approach allowed for the characterization of the reactive species involved in the photocatalytic process.

Characterization

The surface morphologies were characterized using Hitachi S-4800 field emission scanning electron microscope (SEM), transmission electron microscope (TEM) and high-resolution transmission electron microscopy (HRTEM) by a JEOL JEM-2100F microscope. The crystal structures were analyzed by X-ray diffractometer (XRD) using a Bruker D8 Diffractometer. The UV-Vis spectroscopy was performed on the samples using a Shimadzu UV-3600 spectrophotometer. X-ray photoelectron spectra (XPS) were recorded using a Thermo Scientific K-Alpha system equipped with Al-Kα radiation. Additionally, electron spin resonance (ESR) spectroscopy was carried out using a Bruker A300 spectrometer.

Results and discussion

The synthesis involves mixing raw materials in a quartz crucible, followed by heating in a tube furnace at high temperatures to form the Co-doped rutile TiO_2 nanorods (Fig. 1a). Both pure rutile and Co-doped rutile TiO_2 nanorods were prepared using the molten salt method. After purification, the pure TiO_2 nanorods appeared white, while the Co-doped TiO_2 nanorods exhibited a grey-green color (Fig. S1†). In the SEM image (Fig. 1b), the pure TiO_2 nanorods displayed a uniform size and smooth surface. In contrast, the Co-doped TiO_2 exhibited a core/shell nanostructure with an irregular rough surface (Fig. 1c), indicating significant morphological changes due to cobalt doping. To further confirm these morphological changes, both TEM and HRTEM analyses were conducted. The TEM images of a single pure TiO_2 nanorods (Fig. 1d and f) revealed a uniform structure, while the Co-doped TiO_2 showed a distinct core/shell nanostructure (Fig. 1e and g). The HRTEM image of pure TiO_2 nanorods in Fig. 1h exhibited a well-defined crystalline structure with clear lattice fringes along the [001] axis, with interplanar spacing of $d_{001} = 0.32$ nm.[30] After Co doping, the value of the lattice fringes decreased to $d_{001} = 0.20$ nm (Fig. 1i). Compared with the TiO_2 nanorods in Fig. S2,† the EDS elemental mapping image and energy spectra of Co-doped TiO_2 nanorods confirmed the presence of titanium (Ti), oxygen (O), and cobalt (Co) elements (Fig. S3†), further validating the successful doping of cobalt into the TiO_2 nanorods.

The crystallinity and phase purity of the TiO_2 nanorods were confirmed through XRD analysis. As shown in Fig. 2a, the XRD patterns reveal distinct diffraction peaks at 2θ values of 27.5°, 36.1°, 41.2°, 54.3°, and 56.6°, corresponding to the (110), (101), (111), (211), and (220) crystal planes of rutile TiO_2, respectively. The optical properties of both pure TiO_2 and Co-doped TiO_2 nanorods were investigated using UV-Vis absorption spectroscopy. The UV-Vis absorption spectra indicated that the Co-doped TiO_2 nanorods exhibited an additional absorption peak at 600 nm (Fig. 2b). The bandgap values were obtained *via* the Kubelka–Munk function from the corresponding diffuse reflectance spectra.[31] The related curve of $(\alpha h\upsilon)^2$ *versus* photon energy was plotted (Fig. S4†), revealing that the bandgap (E_g) of pure TiO_2 and Co-doped TiO_2 nanorods were 2.99 eV and 3.08 eV, respectively. The specific surface area is critical for increasing the number of sites available for the absorption and

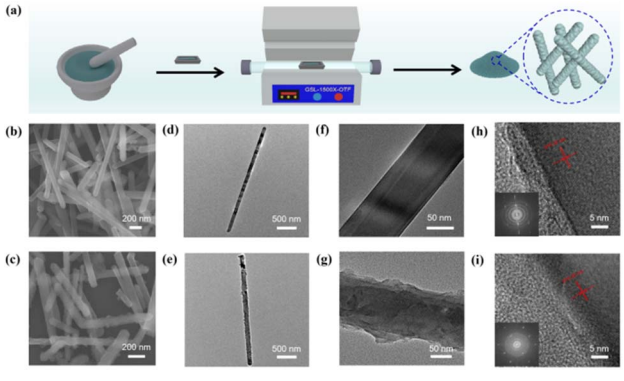

Fig. 1 (a) Schematic representation of the synthesis process for Co-doped TiO_2 nanorods. Characterization of the synthesized TiO_2 nanorods: (b) SEM image, (d) TEM image, and (f and h) HRTEM images of pure TiO_2 nanorods; (c) SEM image, (e) TEM image, and (g and i) HRTEM images of Co-doped TiO_2 nanorods.

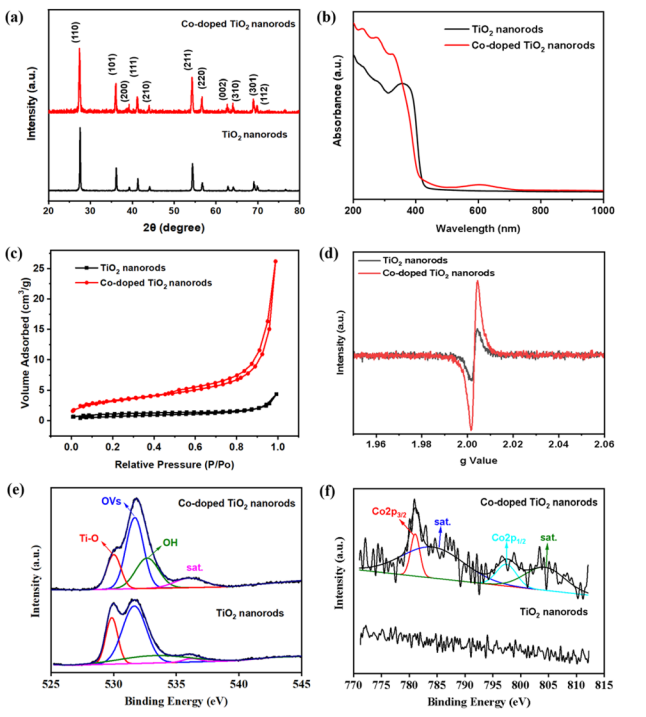

Fig. 2 Characterizations of pure TiO_2 nanorods and Co-doped TiO_2 nanorods: (a) XRD pattern, (b) UV-Vis spectra, (c) N_2 adsorption–desorption isotherms, (d) ESR spectra, (e) O 1s spectra and (f) Co 2p spectra.

© 2025 The Author(s). Published by the Royal Society of Chemistry

Open Access Article. Published on 02 April 2025. Downloaded on 4/29/2026 6:45:28 AM.
This article is licensed under a Creative Commons Attribution-NonCommercial 3.0 Unported Licence.

anchoring of dye molecules during the photodegradation of organic dyes. The specific surface areas of pure and Co-doped TiO_2 nanorods were found to be 15.29 m^2 g^{-1} and 31.99 m^2 g^{-1} (Fig. 2c), respectively.

The ESR spectra of TiO_2 nanorod catalysts were analyzed to investigate the presence of oxygen vacancies (VOs). As shown in Fig. 2d, a strong resonance signal at $g = 2.003$ indicates the existence of VOs within the lattice.[32] Notably, the Co-doped TiO_2 nanorods exhibited a higher concentration of VOs compared to pure TiO_2 nanorods. To further explore the chemical properties of TiO_2 nanorods surface, XPS was performed. The O 1s spectra for Co-doped TiO_2 nanorods, shown in Fig. 2e, revealed distinct peaks at 530.04, 531.73, and 532.71 eV, corresponding to lattice oxygen (Ti–O), oxygen vacancies, and chemisorbed oxygen/hydroxyl groups, respectively.[33] Furthermore, the characteristic peaks in Fig. 2f at binding energies of 797.39 eV for Co $2p_{1/2}$ and 781.06 eV for Co $2p_{3/2}$, are assigned to Co^{2+} species, while the peaks at 803.34 eV and 787.58 eV are indexed to two satellite peaks.[34,35] Additionally, the type and amount of Ti-containing functional groups showed no significant changes after Co-doping (Fig. S5†).

To evaluate the adsorption capabilities of Co-doped rutile TiO_2 nanorods, various organic dyes were used, including Methylene Blue (MB), Neutral Red (NR), Rhodamine B (RhB), Methyl Orange (MO), Brilliant Blue (BB), and Cresol Red (CR). As shown in Fig. 3 and S6a,† the Co-doped TiO_2 nanorods demonstrated 100% adsorption for MB and 75% for NR, while showing negligible adsorption for RhB, MO, BB, and CR. The intensity of the absorption peak of MB at 662 nm gradually decreased (Fig. S6b†). The zeta potential were performed and the results in Fig. S7† showed that the Co-doped TiO_2 nanorods had a peak of −37.6 mV, which indicating the surface of the material was negatively charged in distilled water.[36] To elucidate the selective adsorption of Co-doped TiO_2 for dyes, we conducted DFT calculations to determine the electrostatic potential (ESP), as illustrated in Fig. S8.† Due to electrostatic repulsion, it is reasonable to conclude that MO and BB are not easily adsorbed. If only electrostatic factors were considered, the other four dyes should exhibit adsorption, which contradicts the experimental results. This indicates that the molecular structure could influence the adsorption behavior. To investigate this, we examined the size and structural features of the dyes, as shown in Table S1.† The results indicated that molecules with a more planar conformation, such as MB and NR, were more readily adsorbed onto the photocatalyst surface. In contrast, due to the presence of side chains, CR and RhB can only interact with the surface at a limited number of sites, leading to reduced adsorption capability. Based on the standard curve of MB (Fig. S9†), the calculated adsorption amount of MB increased with the solution concentration (Fig. S10a†), reaching a maximum adsorption capacity of 134.54 mg g^{-1}. Additionally, the adsorption performance of Co-doped TiO_2 nanorods were examined at various pH using MB solution. The optimal adsorption effect was observed at pH = 7, as depicted in Fig. S10b,† indicating that neutral conditions favor the adsorption process.

Before the photocatalytic reaction, the dispersion was stirred in the dark for 90 min to achieve adsorption/desorption

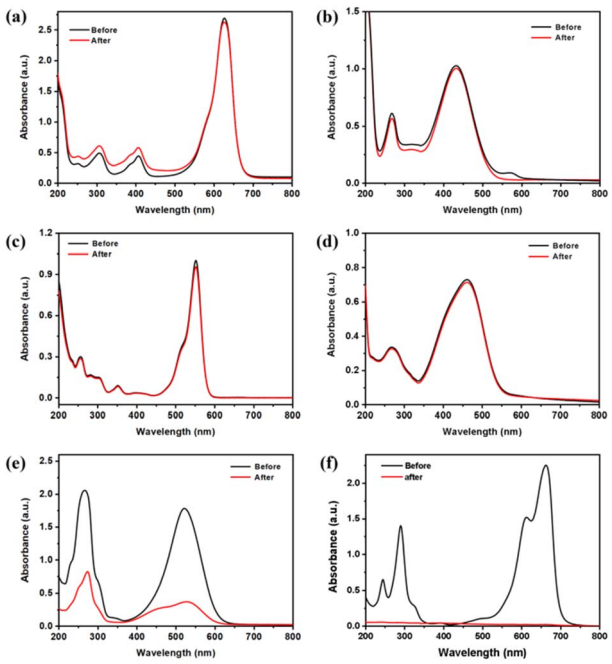

Fig. 3 The UV-Vis absorption curves of different dyes solution before and after adding Co-doped rutile TiO_2 nanorods in the dark at room temperature with 90 min: (a) Brilliant Blue (BB), (b) Cresol Red (CR), (c) Rhodamine B (RhB), (d) Methyl Orange (MO), (e) Neutral Red (NR), (f) Methylene blue (MB) solution.

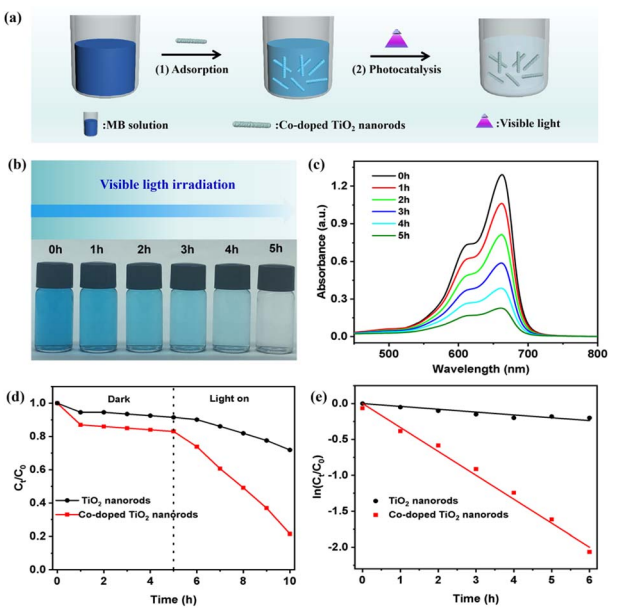

Fig. 4 (a) A schematic representation of the photocatalytic degradation of MB by Co-doped TiO_2 nanorods under visible light, (b) photographs showing the color changes of the MB solution over time, (c) UV-Vis spectra of the degradation of MB during photocatalysis, (d) plots of C_t/C_0 *versus* time under dark and light conditions, and (e) plots of $\ln(C_t/C_0)$ *versus* time for both TiO_2 nanorods and Co-doped TiO_2 nanorods at pH = 7.

Open Access Article. Published on 02 April 2025. Downloaded on 4/29/2026 6:45:28 AM. This article is licensed under a Creative Commons Attribution-NonCommercial 3.0 Unported Licence.

equilibrium. The results showed that, although neutral red dye exhibited high selective adsorption, the UV-Vis spectra revealed no obvious change for neutral red when treated with Co-doped TiO_2 nanorods under visible light irradiation (Fig. S11†). In contrast, the Co-doped TiO_2 nanorods showed efficientl degradation of MB under visible light (Fig. 4a). As demonstrated in Fig. 4b, the color of MB gradually changed from blue to colorless.[37,38] The UV-Vis spectra in Fig. 4c indicated a gradual decrease in the characteristic peak at 662 nm for MB, with the reaction nearing completion after 5 h. According to Fig. 4d, the plot for the dark reaction exhibited almost no decline, while the degradation process of MB under visible light irradiation resulted in a rapid decrease. The calculated apparent reaction rate constant for the Co-doped TiO_2 nanorods was 0.301 min^{-1} (Fig. 4e), which followed first-order kinetic simulation.[39,40] The recoverability and stability were also investigated through repeated photocatalytic experiments. The degradation rates are shown in Fig. S12,† which maintained 60% efficiency over five cycles. Furthermore, the photocatalytic performance of Co-doped TiO_2 nanorods across different pH levels was explored in Fig. S13,† with the highest photocatalytic degradation rate observed under neutral conditions (Fig. S14†). Finally, the catalytic degradation of the MB solution with varying photocatalyst concentrations was investigated. The $\ln(C_t/C_0)$ *versus* time plot in Fig. S15† showed that higher photocatalyst concentrations resulted a higher degradation rate.

To investigate the active species involved in the photocatalytic process of Co-doped TiO_2 nanorods, ESR spectra were measured using spin-trapping reagents.[41] In Fig. 5a, four ESR peaks correspond to $\cdot O_2^-$, with the signal intensities increasing over time. In Fig. 5b, the formation of photogenerated e^- were obviously detected and their concentrations decreased with prolonged light exposure. This observation suggests that the photogenerated electrons can react with molecular oxygen to form superoxide ions.[42] From Fig. 5c, no characteristic peaks were observed in the dark, while characteristic peaks were identified under visible light irradiation, confirming the presence of ·OH in the system.

The proposed photocatalytic mechanism for the degradation of MB by the Co-doped TiO_2 nanorods were shown in Fig. 5d. The 1D Co-doped rutile TiO_2 photocatalyst exhibits three crucial roles in enhancing photocatalytic properties: (1) improved conductivity and increased oxygen vacancies: the incorporation of Co into TiO_2 enhances the conductivity of the catalyst and generates additional oxygen vacancies; (2) facilitated charge separation: the TiO_2 nanorods promote the efficient separation of photogenerated electrons and holes in opposite directions, thereby reducing the recombination of electron–hole pairs;[43] (3) selctive adsorption and photocatalysis: dyes with a positively electrostatic potential and planar conformation for MB are more readily adsorbed and degradated on the negatively charged photocatalyst surface. As a result, the Co-doped TiO_2 nanorods catalysts can effectively generate a higher concentration of reactive oxygen species, including $\cdot O_2^-$ and ·OH, under light irradiation, which contributes to the degradation of MB.

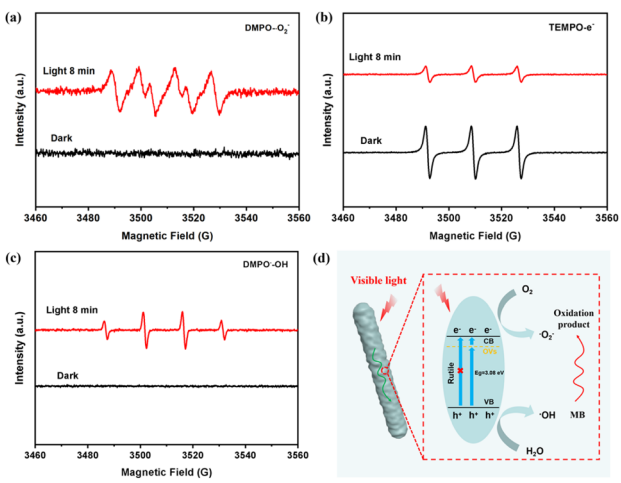

Fig. 5 The ESR spectra obtained from Co-doped rutile TiO_2 nanorods (1.0 mg mL^{-1}) with or without free radical catcher under visible light irradiation: (a) ESR spectra of $\cdot O_2^-$ in methanol captured by DMPO (100 mM), (b) ESR spectra showing the formation of e^- captured in acetonitrile by TEMPO (30 mM), (c) ESR spectra for ·OH in aqueous solution captured by DMPO (100 mM), and (d) a proposed photocatalytic mechanism for the degradation of MB over the photocatalyst under visible light irradiation.

Conclusions

In summary, we have successfully developed a straightforward method for preparing Co-doped rutile TiO_2 nanorods by molten salt flux method. These nanorods exhibited a unique core/shell structure with a rough surface. Both the adsorption experiments and DFT calculations demonstrated that the Co-doped TiO_2 nanorods exhibited a selective adsorption capacity for MB in neutral solution compared to other dyes, which was influenced by the electrostatic potential and molecular structure on the photocatalyst surface. Under visible light irradiation, they achieved a degradation rate constant of 0.301 min^{-1} for MB. The degradation mechanism revealed the generation of reactive species such as $\cdot O_2^-$ and ·OH, which played crucial roles in the photocatalytic process. This study highlights the potential of metal-doped TiO_2 catalysts for environmental protection and the effective treatment of water pollutants, paving the way for further research in this area.

Data availability

The data supporting this article have been included as part of the ESI.†

Conflicts of interest

There are no conflicts to declare.

Acknowledgements

This work is supported by the Natural Science Foundation of Shandong (ZR2022MB106), and the Taizhou Special Support Plan for High-level Talents (Young Talents) (2023NMS01).

© 2025 The Author(s). Published by the Royal Society of Chemistry

Open Access Article. Published on 02 April 2025. Downloaded on 4/29/2026 6:45:28 AM. This article is licensed under a Creative Commons Attribution-NonCommercial 3.0 Unported Licence.

References

1 L. Handojo, D. Pramudita, D. Mangindaan and A. Indarto, *Microorganisms for Sustainability*, 2020, vol. 18, pp. 45–76.
2 Z. Akbari, M. Ghiaci and F. Nezampour, *J. Chem. Eng. Data*, 2018, **63**, 3923–3932.
3 S. Selvaraj, D. S. Patrick, V. S. Manikandan, G. A Vangari, M. K. Mohan and M. Navaneethan, *Surf. Interfaces*, 2024, **51**, 104538.
4 L. Yang, J. L. Ying, Z. Z. Liu, X. L. Xu, Y. Sun, J. N. Yu, G. H. Chen and X. L. Qu, *Mater. Lett.*, 2024, **364**, 136344.
5 H. X. Lü, J. L. Wei, G. X. Tang, Y. S. Chen, Y. H. Huang, R. W. Hu, C. H. Mo, H. M. Zhao, L. Xiang, Y. W. Li, Q. Y. Cai and Q. X. Li, *J. Cleaner Prod.*, 2024, **451**, 141913.
6 Q. J. Liu, L. Shao, Z. Z. Liu, Y. W. Chen, G. Z. Dai and J. L. Ying, *Environ. Technol.*, 2023, **45**, 3600–3611.
7 G. Chen, Y. Wang, Q. Shen, X. Xiong, S. Ren, G. Dai and C. Wu, *Ceram. Int.*, 2020, **46**, 21304–21310.
8 S. Y. Wang, Z. H. Tong, W. J. An, W. Q. Cui and J. S. Hu, *Sep. Purif. Technol.*, 2023, **321**, 124239.
9 L. X. Wu, C. Fu and W. X. Huang, *Phys. Chem. Chem. Phys.*, 2020, **22**, 9875–9909.
10 S. Ding, W. Gan, J. Guo, R. X. Chen, R. Liu, Z. W. Zhao, J. R. Li, M. Zhang and Z. Q. Sun, *J. Mater. Chem. C*, 2024, **12**, 7079–7094.
11 M. X. Tian, Y. M. Yan, Y. Zhang, T. Y. Cui, G. Y. Zhang, J. B. Zhao, Y. Y. Yang and J. H. Jiang, *Inorg. Chem. Commun.*, 2023, **158**, 111578.
12 N. H. Imran, N. G. Fahad, M. K. Al-Hussainawy, H. R. Saud and H. A. K. Kyhoiesh, *Mater. Chem. Phys.*, 2024, **327**, 129888.
13 H. Usui, Y. Domi and H. Sakaguchi, *ACS Appl. Energy Mater.*, 2023, **6**, 4089–4102.
14 B. Fu, Z. J. Wu, S. Cao, K. Guo and L. Y. Piao, *Nanoscale*, 2020, **12**, 4895–4902.
15 A. Mamakhel, J. L. Yu, F. Søndergaard-Pedersen, P. Halda and B. B. Iversen, *Chem. Commun.*, 2020, **56**, 15084–15087.
16 J. Chen, M. L. Guan, X. Zhang and X. Z. Gong, *RSC Adv.*, 2019, **9**, 36615–36620.
17 V. R. Djokić, A. D. Marinković, R. D. Petrović, O. Ersen, S. Zafeiratos, M. Mitrić, C. Ophus, V. R. Radmilović and D. T. Janaćković, *ACS Appl. Mater. Interfaces*, 2020, **12**, 33058–33068.
18 S. Z. K. Yamazaki, M. S. Kutoh, Y. K. Yamazaki, N. M. Yamamoto and M. R. Fujitsuka, *ACS Omega*, 2021, **15**, 31557–31565.
19 S. Bhowmick, R. Sen, C. P. Saini, R. Singhal, L. Walczak, M. Gupta, D. M. Phase and A. Kanjilal, *J. Phys. Chem. C*, 2021, **125**, 4846–4859.
20 M. Q. Lv, D. J. Zheng, M. D. Ye, J. Xiao, W. X. Guo, Y. K. Lai, L. Sun, C. J. Lin and J. Zuo, *Energy Environ. Sci.*, 2013, **6**, 1615–1622.
21 Y. K. Hashemi, M. T. Yaraki, S. Ghanbari, L. H. Saremi and M. H. Givianrad, *Chemosphere*, 2021, **275**, 129903.
22 D. P Wu, J. Guo, H. J. Wang, X. L. Zhang, Y. G. Yang, C. Yang, Z. Y. Gao, Z. C. Wang and K. I. Jiang, *J. Colloid Interface Sci.*, 2021, **585**, 95–107.
23 X. F. Wu, S. Fang, Y. Zheng, J. Sun and K. Lv, *Molecules*, 2016, **21**, 181.
24 D. Mani, R. Tahawy, M. Arivanandhan, R. Jayavel, E. Doustkhah, Ma. Shanmugam and Y. Ide, *Inorg. Chem. Front.*, 2021, **8**, 4423–4430.
25 T. Lu and F. Chen, *J. Comput. Chem.*, 2012, **33**, 580–592.
26 T. Lu and F. W. Chen, *J. Mol. Graphics Modell.*, 2012, **38**, 314–323.
27 J. Zhang and T. Lu, *Phys. Chem. Chem. Phys.*, 2021, **23**, 20323–20328.
28 A. Trocha, O. Impert, A. Katafias and R. V. Eldik, *Polyhedron*, 2021, **210**, 115507.
29 P. Sharma, M. Ganguly and M. Sahu, *RSC Adv.*, 2024, **14**, 14606–14615.
30 B. Liu, H. M. Chen, C. Liu, S. C. Andrews, C. Hahn and P. D. Yang, *J. Am. Chem. Soc.*, 2013, **135**, 9995–9998.
31 J. Xie, S. Wang and F. G. Wang, *Appl. Surf. Sci.*, 2024, **644**, 158709.
32 K. Ramesh, N. Anuradha, A. Siddiqua, J. H. Madhuri, B. V. Kumar and G. Upender, *J. Mol. Struct.*, 2025, **1321**, 140016.
33 W. P. Utomo, H. Wu and Y. H. Ng, *Small*, 2022, **18**, 2200996.
34 D. L. Zhao, C. Q. Ma, J. Li, R. Z. Li, X. Y. Fan, L. C. Zhang, K. Dong, Y. S. Luo, D. D. Zheng, S. J. Sun, Q. Liu, Q. Li, Q. P. Lu and X. P. Sun, *Inorg. Chem. Front.*, 2022, **9**, 6412–6417.
35 Z. F. Zhang, N. Y. Liu, J. W. Wu, J. J. Liu, H. C. Wang, D. W. Pang and J. L. Zheng, *Chem. Phys. Lett.*, 2024, **855**, 141568.
36 M. S. Samuela, S. Joseb, E. Selvarajanc, T. Mathimanid and A. Pugazhendhie, *J. Photochem. Photobiol., B*, 2020, **202**, 111642.
37 Z. Z. Liu, C. Y. Guo, J. L. Ying, X. L. Xu, Y. Xu, Q. J. Liu, G. H. Chen, X. L. Qu, Y. Z. Yue and C. Y. Xue, *Mater. Lett.*, 2025, **379**, 137631.
38 M. G. Kim, J. E. Lee, K. S. Kim, J. M. Kang, J. H. Lee and K. H. Kim, *New J. Chem.*, 2021, **45**, 3485–3497.
39 X. Y. Kang, D. Y. Teng, S. L. Wu, Z. F. Tian, J. Liu, P. F. Li, Y. Ma and C. H. Liang, *J. Colloid Interface Sci.*, 2020, **566**, 265–270.
40 D. Cao, J. Guan, J. C. Du, Q. Sun, J. Ma, J. G. Li, J. T. Liu and G. P. Sheng, *J. Hazard. Mater.*, 2024, **476**, 134956.
41 M. Yu, D. W. Liu, L. C. Wang, J. Xia, J. H. Ren, Y. Q. Fan, X. F. Zhu, J. Wang and K. Xiong, *Appl. Catal. B: Environ.*, 2024, **350**, 123922.
42 L. He, *J. Mater. Sci.: Mater. Electron.*, 2020, **31**, 15522–15529.
43 M. L. Guan, N. Lu, X. Zhang, Q. W. Wang, J. Bao, G. Y. Chen, H. Yu, H. M. Li, J. X. Xia and X. Z. Gong, *Carbon Energy*, 2023, **6**, e420.

© 2025 The Author(s). Published by the Royal Society of Chemistry